

Repeatable self-healing of an epoxy matrix using imidazole initiated polymerization



Kevin R. Hart^{a, c}, Nancy R. Sottos^{b, c}, Scott R. White^{a, c, *}

^a Department of Aerospace Engineering, University of Illinois at Urbana-Champaign, 104 S. Wright St., Urbana, IL 61801, USA

^b Department of Materials Science and Engineering, University of Illinois at Urbana-Champaign, 1304 W. Green St., Urbana, IL 61801, USA

^c Beckman Institute for Advanced Science and Technology, University of Illinois at Urbana-Champaign, 405 N. Mathews Ave., Urbana, IL 61801, USA

ARTICLE INFO

Article history:

Received 29 January 2015

Received in revised form

9 April 2015

Accepted 21 April 2015

Available online 29 April 2015

Keywords:

Self-healing

Latent function

2-Ethyl-4-methylimidazole

ABSTRACT

For the first time, repeatable self-healing was achieved in a cross-linked epoxy polymer by incorporating 2-ethyl-4-methylimidazole (24-EMI) into the matrix as a latent polymerization initiator. Upon material damage and infiltration of liquid EPON 8132 epoxy monomer healing agent into the crack plane, polymerization occurs in the damaged region with a moderate application of heat in the presence of the latent imidazole initiator. Using tapered double cantilever beam (TDCB) fracture testing, greater than 90% recovery of fracture toughness was observed over multiple healing cycles in samples containing 10 wt% 24-EMI, with up to 11 repeat healing cycles possible. The effect of incorporating the imidazole on the host epoxy fracture toughness, complex moduli and glass transition temperature was also investigated. As imidazole concentration increases, a reduction in glass transition temperature and an increase in fracture toughness of the host epoxy is observed.

© 2015 Elsevier Ltd. All rights reserved.

1. Introduction

The use of fiber-reinforced polymer composites in the aerospace, wind energy, automotive and marine sectors has grown over the last few decades, as these materials offer superior specific mechanical properties over traditional structural materials. However, the continuous matrix of these materials typically consists of a brittle thermosetting resin, leaving the composite structure susceptible to crack initiation and growth. To combat the flaw sensitivity of composite materials, self-healing polymers were pioneered to autonomously repair damage in an attempt to minimize maintenance and extend the service life of polymeric composites. A recent review on self-healing materials by Blaiszik et al. [1] broadly characterizes self-healing materials into three separate classes based on the method used to sequester healing agents: microcapsule, microvascular, and intrinsic systems. In this work we explore a new self-healing system which employs aspects of both the

vascular and intrinsic healing schemes for future use in self-healing fiber-reinforced composites.

Vascular based self-healing schemes show promise over capsule-based and intrinsic systems, as vascular systems offer the potential of multiple healing cycles and continuous delivery of agents to large damage volumes. To date, many of the studies on vascular healing in neat polymers have used a two-part, stoichiometrically-based set of healing agents. In polymeric systems containing vasculature, work by Toohey et al. [2] and Hansen et al. [3,4] has demonstrated repeatable recovery of damage in brittle coatings. Additionally, Hamilton et al. [5–7] and Patrick et al. [8] have shown multiple healing cycles of fracture damage in bulk epoxy polymers and polymeric foam materials, respectively. In these studies, stoichiometric mixing of the two agents was required to optimize healing and incomplete mixing of healing components led to reduced performance. Therefore, adequate mixing of the two components in these studies required at least one of the following: complex pumping of the healing agents, mechanically induced mixing, and/or a highly interpenetrated network of channels.

The incorporation of healing agents which require mixing in fiber-reinforced composites is an even more daunting goal. Vascularized fiber-reinforced composites have been fabricated using a variety of techniques including embedment of hollow glass pipettes or glass fibers [9–15], extraction of steel wires [16–19], solder

* Corresponding author. Department of Aerospace Engineering, University of Illinois at Urbana-Champaign, 104 S. Wright St., Urbana, IL 61801, USA. Tel.: +1 217 333 1077.

E-mail address: swhite@illinois.edu (S.R. White).

URL: <http://www.autonomic.uiuc.edu>

removal [20–22], or vaporization of sacrificial components [23,24]. However, integrating vascular networks in fiber-reinforced composites that are dense enough to ensure in-situ stoichiometric mixing, yet sparse enough to leave the reinforcing architecture and mechanical properties of the composite unaltered is a research challenge that has not yet been achieved. As a result, many studies have used pre-mixed healing agents or complex external control systems to achieve adequate mixing of the two constituents for healing, severely limiting autonomy of the repair system.

In addition to two-part stoichiometrically-based systems for healing, other authors have investigated two-part reversible cross-linking reactions or one-part catalyst/initiator based polymerization schemes. Reversible cross-linking via the Diels–Alder and retro-Diels–Alder reaction has shown success healing cracks in compact tension specimens, flexure specimens, short-beam shear specimens, single fiber pull-out specimens and coatings [25–30]. In this scheme, liquid maleimide dienophiles reacted in the crack plane with embedded furan dienes in the matrix to facilitate healing. However, these reversible cross-linking reactions require very small crack separations and/or external crack closing forces to bring the fractured surfaces into intimate contact, limiting their potential use in vascular self-healing systems which target healing of large damage volumes. In one-part catalytic schemes, the ring opening metathesis polymerization (ROMP) of dicyclopentadiene has been utilized in microcapsule based healing systems in a variety of polymers to demonstrate recovery of: compression after impact strength in composites [31], glass fiber/matrix interfaces [32], glass/epoxy composite tensile and shear properties [33,34], and fracture damage in polymer coatings [35], bulk polymers [36], adhesives [37,38] and composites [39,40]. Additionally, initiator based epoxy/imidazole [41–44], epoxy/mercaptan [45], and epoxy/lewis acid [46] polymerization schemes have been explored for healing of impact damage and mode I fracture in epoxy and composite systems. Imidazole based anionic polymerization schemes demonstrate a particularly high potential for application in self-healing materials. Imidazoles are commercially available, easily chemically tailored through ligand attachment, stable in ambient conditions, commonly used as epoxy polymerizing agents in industry, and inexpensive relative to other catalysts and initiators used in self-healing systems.

The anionic polymerization of various imidazoles with epoxide monomers has been previously described by Heise and Martin [47–49]. Unlike catalytic polymerization reactions, the imidazole initiator reacts with the epoxide groups and is consumed to form a backbone for anionic polymerization. Yin et al. [41–43] have explored imidazole systems for use in self-healing materials by utilizing a solid copper-bromide-imidazole complex as a latent initiator embedded in a host epoxy matrix/composite. Using that system, authors demonstrated 111% recovery of mode I fracture in single edge notch beam specimens of pure epoxy [41], 78% recovery of mode I critical strain energy release rate in E-glass/epoxy double cantilever beam specimens [42], and 94% recovery of compression after impact strength in E-glass/epoxy composites [43]. However, healing temperatures of up to 140 °C were required, and healing events were limited to a single cycle. It is our aim to expand upon the success of the imidazole system to demonstrate multiple healing events in a composite specimen, while minimizing the thermal requirements of healing observed in previous self-healing studies.

In this paper, we present an alternative method of repeatable self-repair in an epoxy based polymer system using imidazole initiated polymerization of an epoxy resin. Latent functionality is built into a typical epoxy matrix by the addition of liquid 2-ethyl-4-methylimidazole (24-EMI) into the matrix material during processing. Healing is achieved by the injection of liquid

epoxy monomer into damaged regions where polymerization of the healing agent monomer is initiated thermally in the presence of the latent imidazole. Polymerization kinetics and chemical mechanisms of the healing reaction are evaluated using dynamic scanning calorimetry (DSC) and Raman spectroscopy, while dynamic mechanical analysis (DMA) is utilized to determine the effect of imidazole incorporation on mechanical properties and glass transition temperature of the imidazole laden epoxy matrix host. Healing performance is assessed using bulk epoxy tapered-double-cantilever-beam (TDCB) specimens while scanning electron fractography is employed to observe healed material in previously damaged regions. The successful demonstration of this healing system in bulk epoxy will open pathways for one-part microvascular healing in fiber-reinforced composites.

2. Experimental methods

2.1. Materials

Liquid epoxy monomers EPON 862 (diglycidyl ether of bisphenol F) and EPON 8132 (1,2-epoxy-3-chloropropane) as well as cycloaliphatic amine curing agent Epikure 3300 were obtained from Miller–Stephenson (Morton Grove, IL) and used as-received. The EPON 862/Epikure 3300 system was selected as the matrix material because of its precedence in prior work by Esser Kahn et al. which was the first to demonstrate the vaporization of sacrificial components procedure for the creation of three-dimensionally woven microvascular composites [23]. EPON 8132 was selected as the healing agent monomer because of its precedence as a low viscosity, low molecular weight healing agent component in other self-healing systems [2,3,5,6,24]. The initiator 2-ethyl-4-methylimidazole (24-EMI) was obtained from Sigma–Aldrich (Saint Louis, MO) and used in liquid form as-received.

2.2. Manufacturing and healing protocols

TDCB fracture specimens were prepared by mixing 24-EMI with a stoichiometric ratio of EPON 862/Epikure 3300 (100:22.7 by weight), degassing under vacuum at room temperature for 15 min and pouring the mixture into silicone rubber molds. Samples were then placed in a convection oven and cured at the manufacturer's recommended cure of 4 h at 30 °C, plus an additional 90 min at 82 °C, plus an additional 90 min at 150 °C. Although the imidazole does react with the EPON 862, the kinetics at 30 °C are slow relative to the primary epoxy/amine matrix reaction. As such, it was critical to gel and solidify the matrix epoxy first at 30 °C in order to minimize reaction of the imidazole and the matrix epoxy before elevating the temperature to fully cure the sample. Following the cure cycle, samples were post cured for 24 h in a vacuum oven at 200 °C in order to simulate the vascularization process described by Esser-Kahn et al. [23].

2.3. Fracture and healing tests

Short groove TDCB specimens [50] were used to evaluate fracture toughness and healing performance. Prior to testing, a small pre-crack was introduced into the center groove of the TDCB sample by lightly tapping a razor blade into the front of the fluted region. Testing was carried out on a load frame in displacement control at 5 μm/s until the crack propagated to the end of the grooved region. Samples were then unloaded and removed from the machine. Healing was accomplished by carefully injecting approximately 15 μL of EPON 8132 healing agent into the crack plane along the sample edge. After wicking into the

crack plane, excess healing agent was removed from the side of the sample and then placed in an oven for a prescribed healing time and temperature. Control samples were not injected with healing agent after fracture, but were subjected to the same thermal healing conditions. In samples capable of multiple healing cycles, healing agent injection, thermal treatment, and fracture testing were repeated until no further recovery of fracture toughness was observed. Fracture toughness was calculated using

$$K_{IC} = 2P_C \sqrt{\frac{m}{b_n b}} = \alpha P_C \quad (1)$$

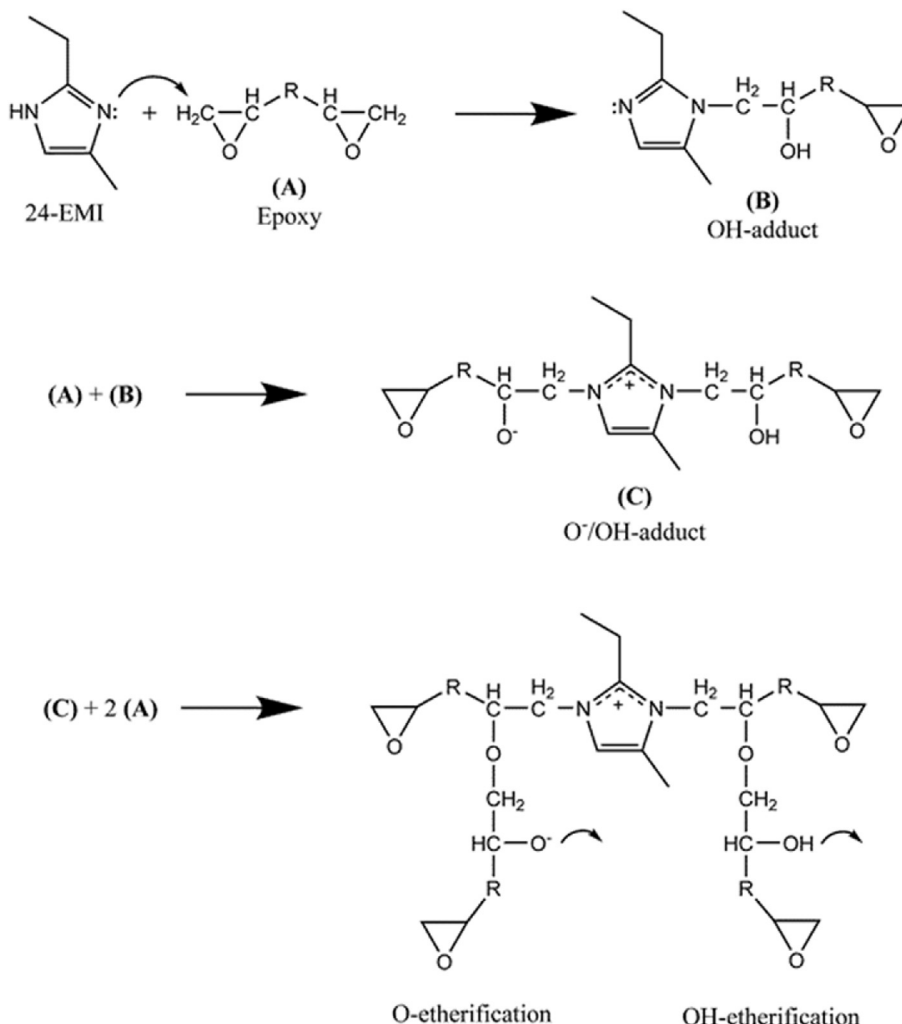
where K_{IC} is the mode I critical fracture toughness, P_C is the critical load at fracture, b_n is the width of the fracture plane (2.5 mm), b is the thickness of the sample (6.25 mm), α is a constant, and m is a geometric constant calculated from experiments using

$$m = \frac{Eb}{8} \frac{dC}{da} \quad (2)$$

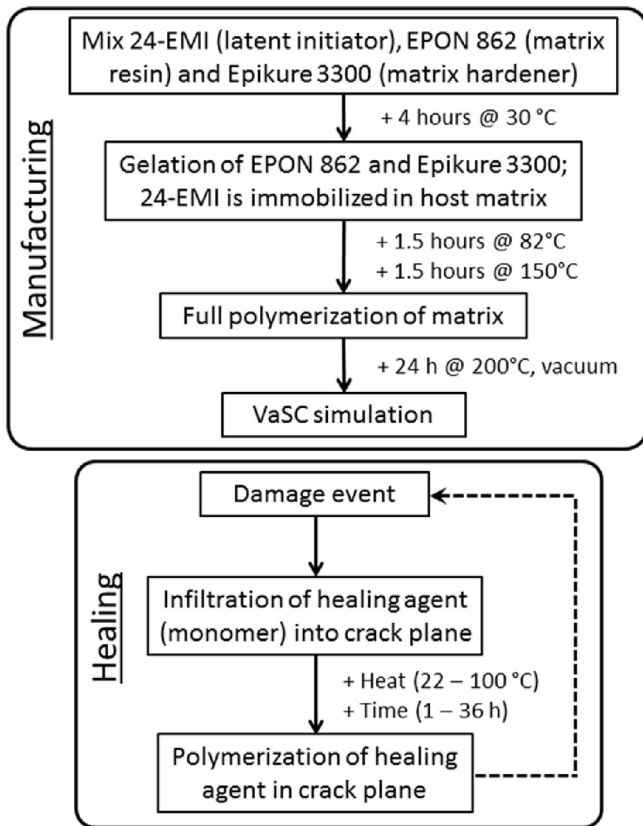
where E is the elastic modulus of the polymer and dC/da is the change in compliance per unit crack advance [50].

2.4. Differential scanning calorimetry

Polymerization kinetics of the reaction between the EPON 8132 healing agent and 24-EMI (Scheme 1) were investigated using dynamic scanning calorimetry (DSC). Samples (Type I) were prepared by mixing 0, 2, 5, or 10 wt% 24-EMI with EPON 8132 healing agent. Approximately 10 mL of the mixture was then degassed for 20 min before loading into the DSC. Another type of sample was also prepared to more closely mimic *in-situ* healing conditions. In these samples (Type II), shavings from a cast polymer block of EPON 862/Epikure 3300 containing 10 wt% 24-EMI were collected by sanding the polymer block against 80 grit sandpaper and harvesting the particles (ca. 10–150 μm in size). EPON 8132 monomer was then added to the solid shavings to yield suspensions containing 0, 2, 5, or 10 wt% imidazole/healing agent equivalent. After fabrication, both sample types were stored in a freezer at -20°C . For testing, approximately 15 mg of a sample was added to an aluminum sample pan which was then hermetically sealed and loaded into the DSC. Samples undergoing dynamic scans were ramped from 0°C to 300°C at a rate of $5^\circ\text{C}/\text{min}$. Those undergoing isothermal scans were equilibrated at 40°C then ramped to the target isothermal temperature at a rate of $60^\circ\text{C}/\text{min}$ and held for the duration of the test. All DSC experiments were performed in a nitrogen environment on a TA Instruments Q20 Differential Scanning Calorimeter, thermally calibrated with Indium standards.



Scheme 1. Reaction mechanism for the curing of epoxy monomers with 24-EMI.



Scheme 2. Manufacturing and healing protocols for self-healing epoxy specimens.

2.5. Dynamic mechanical analysis

Glass transition temperature and viscoelastic properties were evaluated using dynamic mechanical analysis (DMA). To prepare specimens, 24-EMI was mixed into a stoichiometric ratio of EPON 862/Epikure 3300 (100:22.7 by weight), degassed under vacuum at room temperature for fifteen minutes, cast into 2 mm thick sheets between teflon coated glass plates, then cured and post-cured as described in Scheme 2. Rectangular blocks measuring $14 \times 5 \times 2$ mm were then cut and tested in three-point flexure (10 mm span) on a TA Instruments RSA III Dynamic Mechanical Analyzer in air according to ASTM D7028. Samples were tested in strain control (0.5%) at a constant frequency of 1 Hz while ramped in temperature from 25 to 250 °C at 5 °C/min.

2.6. Scanning electron microscope fractography

The fracture surfaces of healed and virgin TDCB specimens were imaged using scanning electron microscopy. Half of a fully fractured TDCB specimen was sectioned to isolate the crack plane, triple rinsed with ethyl alcohol to remove excess healing agent monomer, and dried in air. The sample was then sputter coated with

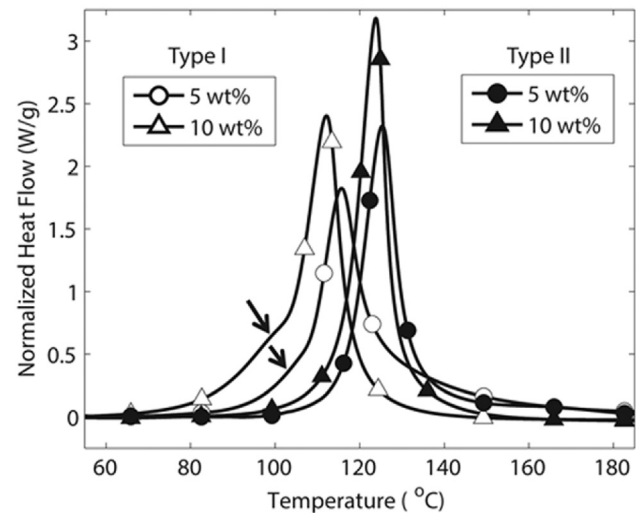


Fig. 1. Representative heat flow vs temperature curves for dynamic DSC testing of type I (EPON 8132 monomer + 24-EMI) and Type II (EPON 8132 monomer + 24-EMI in epoxy matrix) samples. Arrows indicate exothermic rise from adduct formation in type I samples.

gold–palladium and imaged using a secondary electron detector on a Philips XL30 ESEM-FEG scanning electron microscope.

2.7. Raman spectrography

Raman spectra were gathered on a variety of specimens in order to confirm the proposed healing mechanism. Specimens were prepared according to the compositions and curing conditions detailed in Table 1. After curing, samples were cut into $50 \times 50 \times 2$ mm thick squares and sanded using 400 grit polishing paper. Samples were then subjected to healing conditions by placing them into a bath of EPON 8132 healing agent and heating to 100 °C for 1 h to facilitate polymerization of the healing agent on the sample surface via latent imidazole initiation (for self-healing specimens). Before gathering Raman spectra, all samples were triple rinsed with ethanol and dried at room temperature in air.

Stokes Raman scattering was measured using a Horiba model LabRAM HR 3D Raman confocal imaging microscope with an affixed Andor Newton DU970P EMCCD camera (1600×200 pixels), $100\times$ objective, and 785 nm near-IR laser. Hardware was controlled and spectra were analyzed with LabSpec 5 (v5.78.24) spectroscopy software. Single spot scans were performed and intensity counts of Raman shifts between 500 cm^{-1} and 4000 cm^{-1} were collected.

3. Results and discussion

3.1. Polymerization kinetics

3.1.1. Dynamic DSC scans

A representative graph of heat flow as a function of temperature recorded during dynamic DSC scans of type I

Table 1
Specifications for samples examined during Raman spectroscopy.

Designation	Type	Composition (ratio by mass)	Curing schedule	Healing schedule
Self-healing I	Epoxy with imidazole	Epon 862 + Epikure 3300 (100:22.7)	4 h 35 °C + 1.5 h 82 °C + 1.5 h 150 °C	n/a
Self-healing II	Epoxy with imidazole	Epon 862 + Epikure 3300 (100:22.7)	4 h 35 °C + 1.5 h 82 °C + 1.5 h 150 °C	1 h, 100 °C
Control I	Neat epoxy	Epon 862 + Epikure 3300 + 10 wt% 24-EMI (100:22.7:10)	4 h 35 °C + 1.5 h 82 °C + 1.5 h 150 °C	n/a
Control II	Neat epoxy	Epon 862 + Epikure 3300 + 10 wt% 24-EMI (100:22.7:10)	4 h 35 °C + 1.5 h 82 °C + 1.5 h 150 °C	1 h, 100 °C
Pre-mixed healing agent	Pre-mixed imidazole and epoxy monomer	Epon 8132 + 24-EMI (100:10)	1 h, 100 °C	n/a

Table 2

Heat of polymerization as a function of 24-EMI content calculated from dynamic DSC scans of type I and type II epoxy/imidazole samples.

24-EMI content, wt%	Heat of polymerization, J/g	
	Type I ^a	Type II ^b
2	284	277
5	489	404
10	464	417

^a Type I sample: EPON 8132 monomer + 24-EMI.

^b Type II sample: EPON 8132 monomer + (EPON 862/Epikure 3300)/24-EMI epoxy shavings.

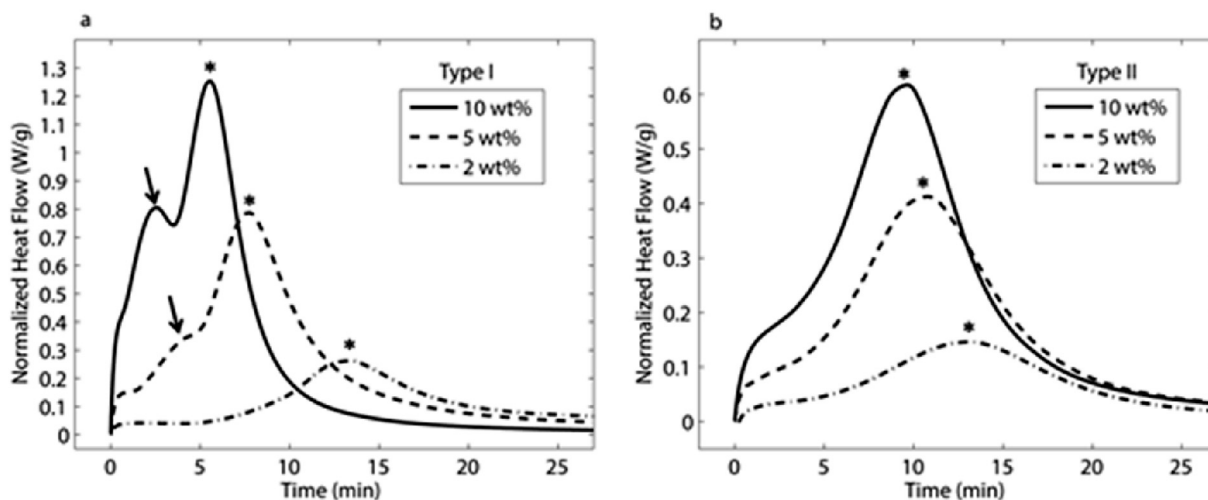


Fig. 2. Isothermal DSC scans at 100 °C of (a) type I and (b) type II samples containing 2, 5, and 10 wt% 24-EMI. Adduct formation (arrow) is observed before etherification (*) in type I samples, but is absent in type II samples.

(healing agent monomer + imidazole) and type II (healing agent monomer + imidazole in matrix) samples containing 5 and 10 wt% imidazole is provided in Fig. 1. In type I samples, polymerization initiates at lower temperatures compared to type II samples where the initiator must first be extracted from the epoxy matrix before reacting with the monomer. Also, a shoulder in the exothermic peak is observed in type I samples between 100 °C and 120 °C that is absent in type II samples. This shoulder to the main exothermic peak was first observed by Heise and Martin [48] and is attributed

$$H_T = \frac{1}{m} \int_{t(T=25^\circ\text{C})}^{t(T=300^\circ\text{C})} [Q(T(t)) - y(t)] dt \quad (3)$$

where H_T is the normalized total heat of reaction, m is the mass of the monomer, t is time, T is temperature, $Q(T(t))$ is the recorded heat flow, and $y(t)$ is a linear baseline of the function $Q(T(t))$ between 25 and 300 °C. Total heat of polymerization for all tests is provided in Table 2. Heat of polymerization of type I samples is

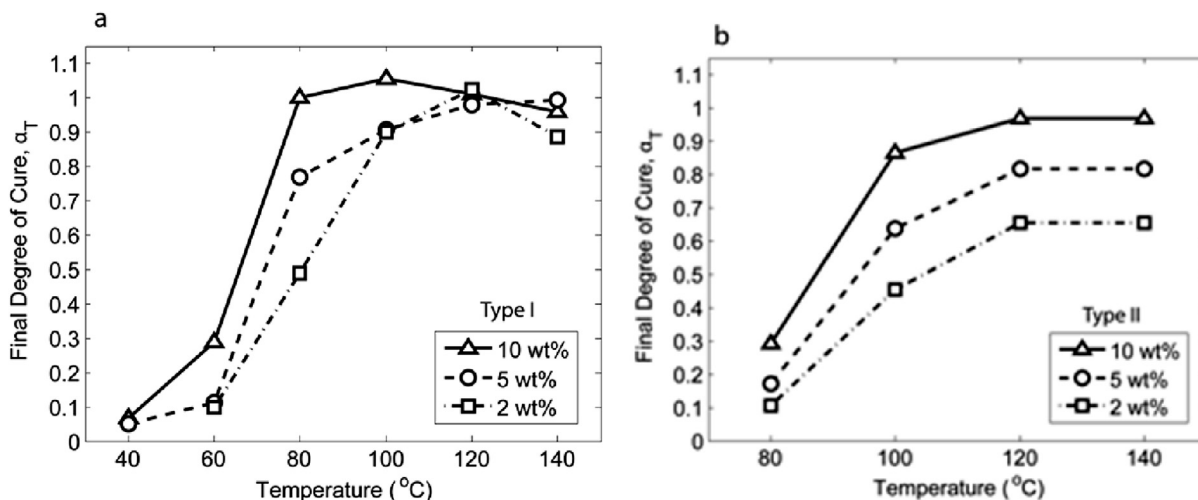


Fig. 3. Final degree of cure (α_T) as a function of isothermal temperature from DSC testing of (a) type I and (b) type II samples containing various amounts of 24-EMI.

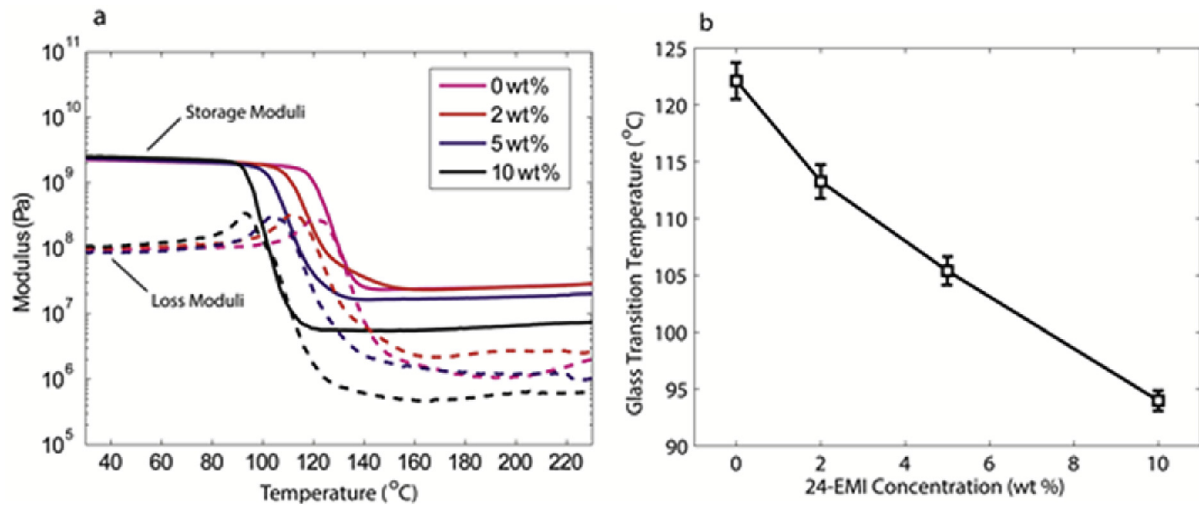


Fig. 4. (a) Storage and loss moduli and (b) glass transition temperature from DMA testing of epoxy specimens containing various concentrations of 24-EMI. Error bars represent one standard deviation.

consistently greater than that of type II samples due to the adduct formation reactions which are absent in type II samples. Additionally, samples containing 2 wt% imidazole display reduced heat of polymerization compared to samples containing 5 and 10 wt% additive. Reductions in the heat of polymerization at low imidazole concentrations have been observed previously in the literature [48,49] and are attributed to a lack of initiation sites created during adduct formation. Because adequate adduct formation is critical to provide the backbone and growth of the polymer, limited adduct formation severely restricts etherification chain growth in samples with low imidazole concentrations.

3.1.2. Isothermal DSC scans

Isothermal DSC scans of type I and type II samples are displayed in Fig. 2. As imidazole concentration is increased in both sample types, polymerization proceeds more quickly and the maximum heat flow is greater. In type I samples containing 5 and 10 wt% imidazole, a small peak is observed before the main exothermic peak. This peak is attributed to the adduct reactions which occur before the main etherification reaction, as described by Heise and Martin [48]. This peak is absent in type II samples, indicating that the adduct reaction occurred in these samples during initial epoxy matrix formation.

Total degree of polymerization from isothermal testing of type I and type II samples is calculated using

$$\alpha_T = \frac{H_T^{Iso}}{H_T^{Dyn}} \quad (4)$$

and plotted against isothermal scanning temperature in Fig. 3, where α_T is the final degree of cure of the samples, H_T^{Iso} is the total normalized heat of reaction in the isothermal scan, and H_T^{Dyn} is the total heat of reaction calculated from the dynamic scan of the same condition. In type I samples containing 10 wt% imidazole, approximately 100% polymerization is realized in one hour at temperatures of 80 °C and higher. Type I samples containing 2 and 5 wt% imidazole also demonstrate >90% polymerization at temperatures of 100 °C and above. Type II samples plateau in their final degree of cure, depending on the initiator concentration present since monomer access to the imidazole is more restricted in type II samples.

3.2. DMA testing

Storage and loss moduli from DMA testing of polymers manufactured with 0, 2, 5, and 10 wt% imidazole are plotted in Fig. 4a. Glass transition temperature was calculated following ASTM D7028 as the intersection point between the linear region before transition and the tangent line to the inflection point during transition and is plotted as a function of imidazole concentration in Fig. 4b. While the introduction of the imidazole into the host matrix has negligible effect on the complex moduli below T_g , the glass transition temperature and post transition moduli above T_g are both reduced with increasing imidazole concentration.

3.3. Fracture testing

Fig. 5 shows representative load/displacement curves for a TDCB specimen healed over multiple healing cycles. In all tests, peak

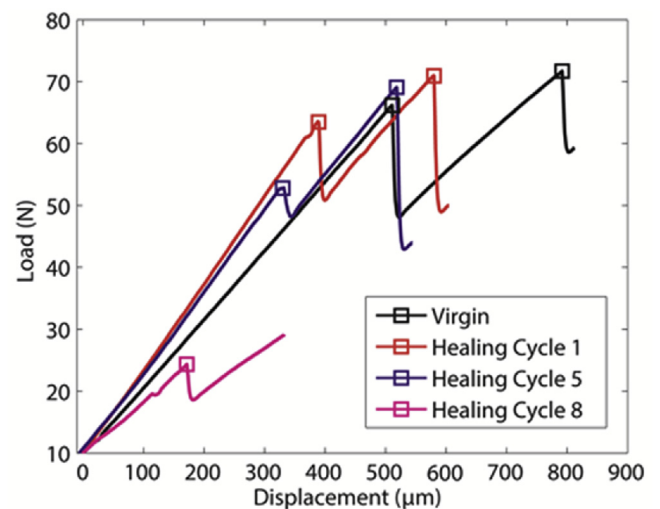


Fig. 5. Representative load/displacement curves of a TDCB fracture specimen containing 10 wt% 24-EMI tested over multiple self-healing cycles. In each healing cycle, EPON 8132 monomer was injected into the crack plane and the sample was heated to 100 °C for one hour. Boxes (□) represent peak loads during crack propagation used in the calculation of fracture toughness.

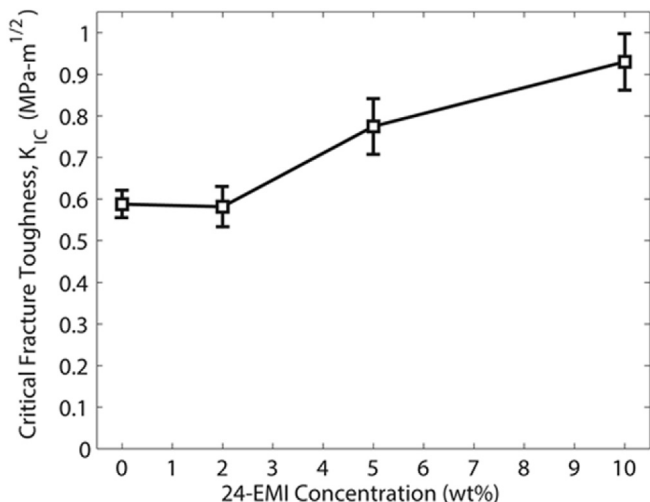


Fig. 6. Critical mode I fracture toughness as a function of 24-EMI concentration in the host epoxy matrix. Error bars represent one standard deviation.

loads were easily identified because of the elastic, brittle nature of the polymer. Since multiple fracture events were observed for each sample during testing, the critical load (P_C) used to calculate fracture toughness was taken as the average of the peak loads at fracture for each individual test. The initial stiffness of virgin tests was lower than healed tests because of the short pre-crack required in virgin tests to initiate crack propagation. Later, healing agents infiltrate the pre-cracked region and restore the integrity of the pre-crack, leading to slightly increased stiffness. The change in stiffness observed here between virgin and healed specimens has no effect on the measured fracture toughness [50].

Healing efficiency is reported as a ratio between the healed and virgin fracture toughness of the sample, which may be reduced in the case of a TDCB specimen to the ratio of peak loads at fracture as:

$$\eta_i = \frac{(K_{IC}^{Healed})_i}{K_{IC}^{Virgin}} = \frac{(P_C^{Healed})_i}{P_C^{Virgin}} \quad (5)$$

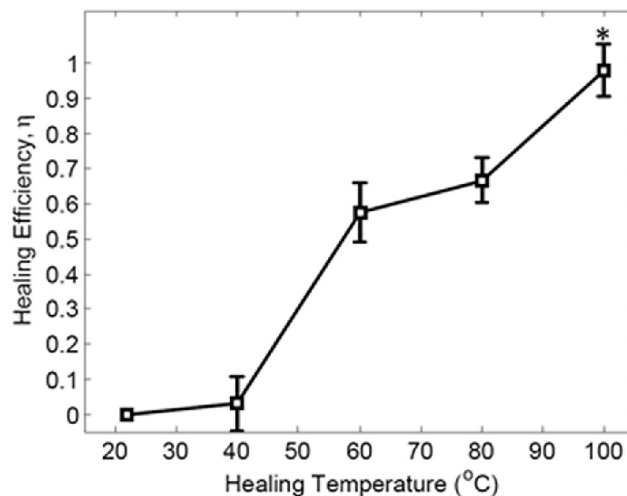


Fig. 8. Healing efficiency as a function of healing temperature for specimens containing 10 wt% 24-EMI healed for 36 h. Reference point at 100 °C (*) was healed for only one hour. Errors bars represent one standard deviation.

where η_i is the healing efficiency, $(K_{IC}^{Healed})_i$ and $(P_C^{Healed})_i$ are the healed fracture toughness and average peak load of the i th healing cycle, and K_{IC}^{Virgin} and P_C^{Virgin} are the fracture toughness and average peak loads of the virgin test.

3.3.1. Virgin fracture toughness

In virgin tests of samples containing 0, 2, 5, or 10 wt% imidazole, fracture toughness increased with increasing initiator concentration (Fig. 6). Most noticeably, samples containing 10 wt% imidazole showed a 58% enhancement in fracture toughness over samples without any additive, increasing from 0.588 to 0.930 MPa-m^{1/2}.

3.3.2. Effect of varying imidazole concentration on healing efficiency

Healing efficiency for TDCB specimens is plotted in Fig. 7a as a function of healing cycle for a healing cycle of 1 h at 100 °C. After the first healing cycle, samples containing 2, 5, and 10 wt% imidazole demonstrated 16%, 65%, and 98% healing efficiency,

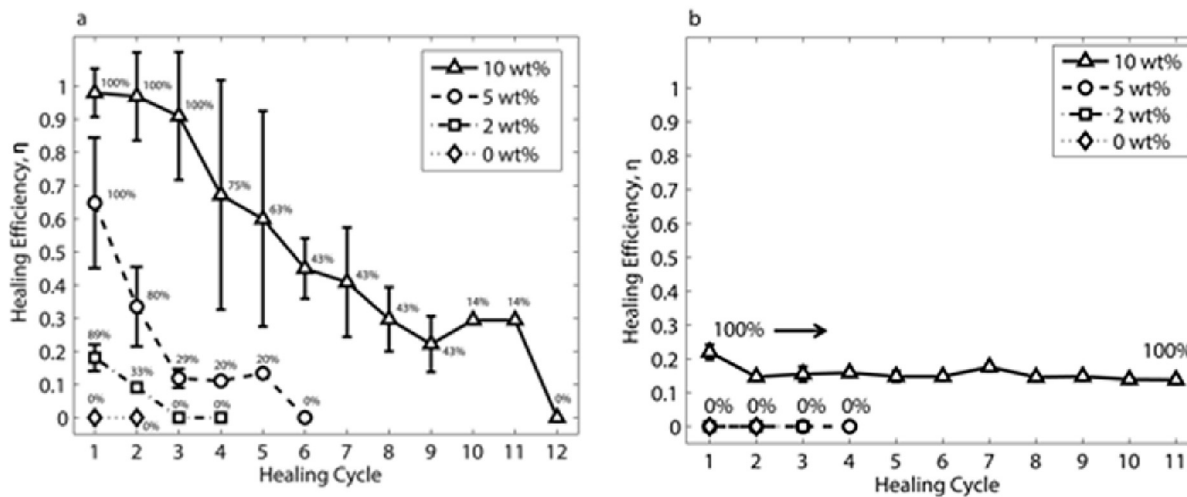


Fig. 7. Healing efficiency (η) as a function of healing cycle for samples containing 0–10 wt% 24-EMI. (a) Self-healing samples with injected EPON 8132 monomer. (b) Control specimens in which no healing agent was injected. All samples were subjected to a 1 h healing cycle at 100 °C between cycles. Percentages listed indicate the fraction of specimens tested at that condition which demonstrated non-zero healing. Samples demonstrating no healing were not included in the calculation of healing efficiency. All error bars represent one standard deviation.

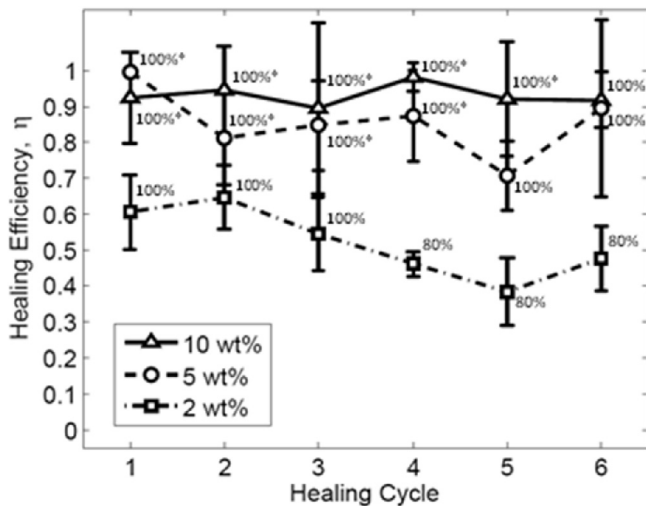


Fig. 9. Healing efficiency plotted over multiple healing cycles for reference specimens healed using pre-mixed healing agent of EPON 8132 + 24-EMI at various concentrations. All samples were healed for 1 h at 100 °C. Percentages listed indicate the fraction of specimens tested at the given condition which demonstrated non-zero healing. Starred data (*) indicate that at least one data point in the series demonstrated greater than 100% healing efficiency and was truncated to 100% during analysis. All error bars represent one standard deviation.

respectively, while samples containing no imidazole did not show any recovery of fracture toughness. Healing efficiencies then decreased with increasing healing cycles, falling to zero at cycles 3, 6, and 12 for samples containing 2, 5, and 10 wt% imidazole, respectively. As new (healed) polymer accumulated in the crack plane after each healing cycle, access to the latent imidazole initiator in the host epoxy matrix was increasingly hindered until further polymerization became impossible. Reduced healing performance of samples containing 2 and 5 wt% is attributed to incomplete polymerization of healed material in the crack plane. From isothermal DSC testing at 100 °C, the final degree of cure for the epoxy monomer in samples containing 2 and 5 wt% imidazole is 45% and 64%, respectively, after 1 h, whereas samples with 10 wt% imidazole show >85% cure.

In control samples subject to a 100 °C thermal healing cycle for one hour, but containing no healing agent, minor recovery in fracture toughness (~15–20%) was repeatedly observed in samples

containing 10 wt% imidazole (Fig. 7b). In contrast, no recovery of toughness was observed in samples containing 0, 2, or 5 wt% imidazole. The healing temperature (100 °C) is greater than T_g for 10 wt% imidazole samples (94 °C), but less than T_g for 0, 2, and 5 wt% samples (105–123 °C). Consequently, the recovery in control specimens containing 10 wt% imidazole is attributed to deformation, flow, and re-vitrification of the material at the crack plane upon cooling from above the materials' glass transition temperature as similarly observed in other studies on epoxy-based materials by Outwater and Gerry [51] and Rahmathullah and Palmese [52].

3.3.3. Effect of post cure thermal treatment

TDCB fracture specimens containing either 0 wt% or 10 wt% initiator were fabricated as described in Scheme 1 but without the 200 °C, 24 h post cure, to test the effects of the post cure thermal treatment on fracture performance. Three samples of each type were tested. Samples containing 10 wt% imidazole had a virgin fracture toughness of $0.737 \pm 0.078 \text{ MPa}\cdot\text{m}^{1/2}$ (with treatment: $0.766 \pm 0.056 \text{ MPa}\cdot\text{m}^{1/2}$) and a healed fracture toughness of $0.760 \pm 0.019 \text{ MPa}\cdot\text{m}^{1/2}$ ($0.755 \pm 0.070 \text{ MPa}\cdot\text{m}^{1/2}$) after one healing cycle. Samples containing 0 wt% imidazole had a virgin fracture toughness of $0.460 \pm 0.007 \text{ MPa}\cdot\text{m}^{1/2}$ ($0.484 \pm 0.024 \text{ MPa}\cdot\text{m}^{1/2}$) and showed no recovery of fracture toughness after one healing cycle. Data indicates that the post cure thermal treatment has no significant effect on the fracture and healing behavior of the material.

3.3.4. Effects of varying healing temperature on healing efficiency

Fig. 8 shows the effect of healing temperature on healing efficiency in TDCB specimens containing 10 wt% imidazole healed for 36 h. While healing efficiency at 100 °C was 98%, as the healing temperature was reduced, the healing efficiency also decreased. Moderate levels of healing (ca. 60%) were obtained at or above 60 °C, but healing efficiency dropped precipitously to near zero at 40 °C and 22 °C. Therefore, to achieve appreciable healing over a 36 h healing cycle, a minimum temperature of 60 °C is required.

3.3.5. Effects of imidazole depletion on repeat self-healing capability

A series of reference test cases were carried out in which the epoxy healing agent monomer (EPON 8132) was pre-mixed with the imidazole before injecting into fractured TDCB specimens. For these reference tests, access to imidazole initiator was unhindered

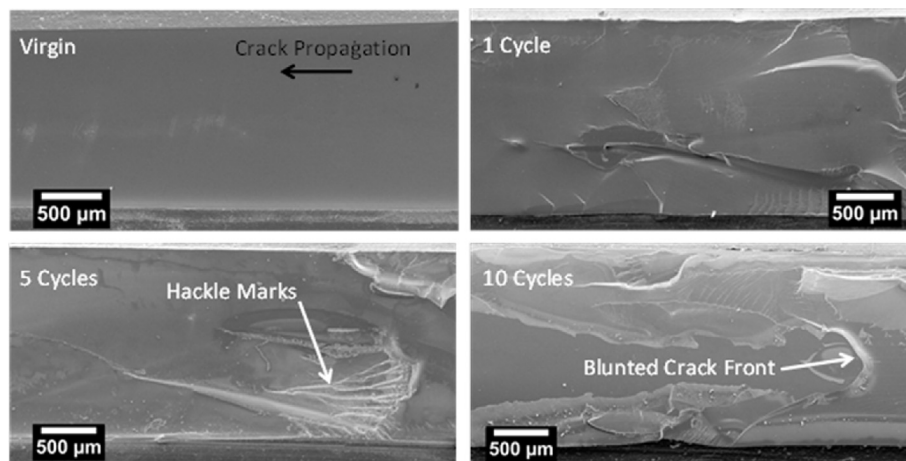


Fig. 10. Fracture surfaces of self-healing TDCB specimens containing 10 wt% 24-EMI after 0 (virgin), 1, 5, and 10 healing cycles. Virgin fracture surfaces appear clean and glassy, indicating brittle failure. As the number of healing cycles increased, more polymer build-up and crack plane tortuosity (hackle marks/crack blunting) was observed, confirming the presence of healed material. Crack propagation is right to left in all images.

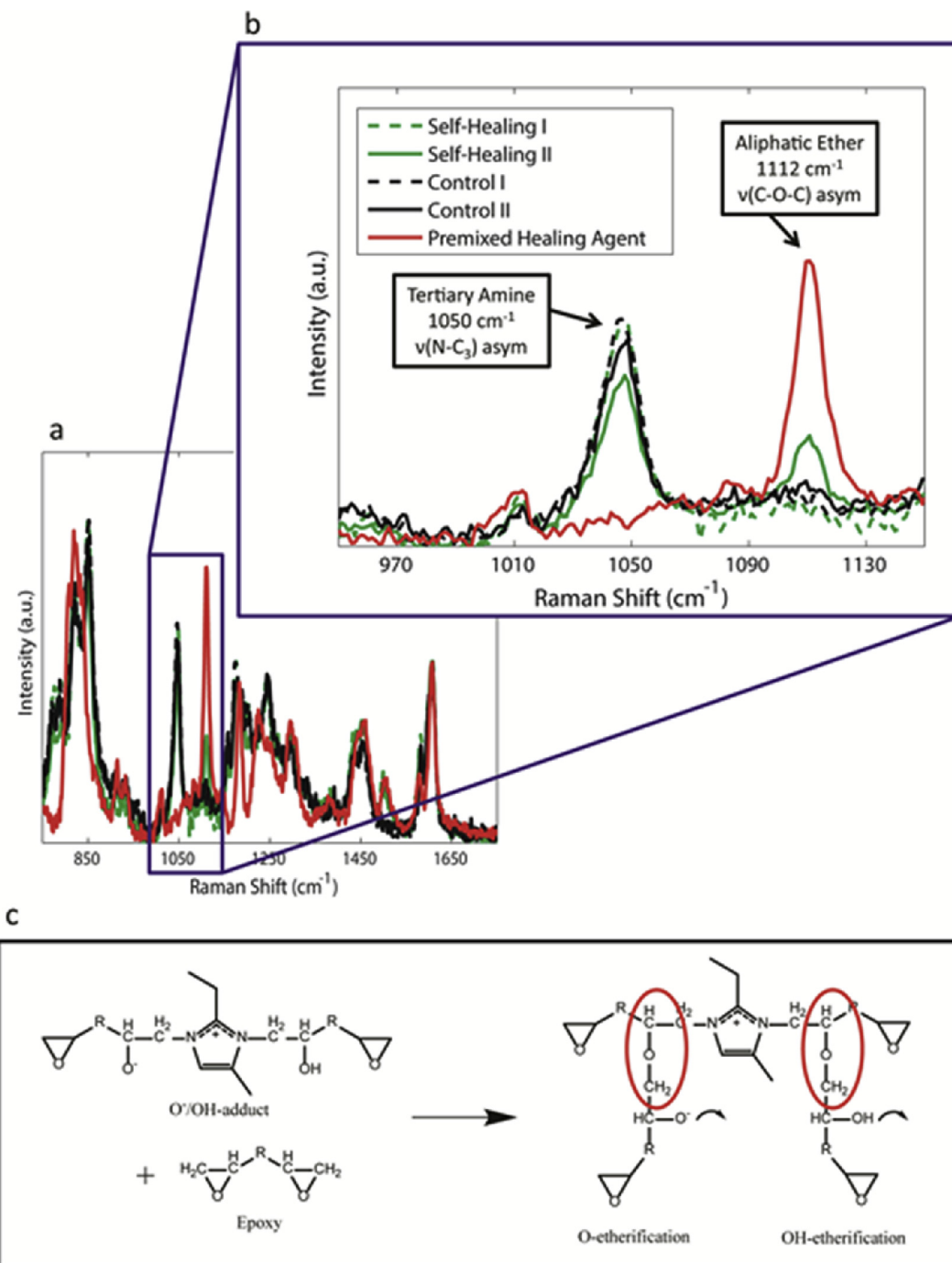


Fig. 11. Raman shift of control, self-healing, and reference premixed epoxy polymers between 750–1750 cm⁻¹ (a) and 950–1150 cm⁻¹ (b). Emergence of a peak at 1112 cm⁻¹ in the self-healing II specimen corresponds to asymmetric stretch of an aliphatic ether bond (red ovals) formed during the healing reaction (c). (For interpretation of the references to color in this figure legend, the reader is referred to the web version of this article.)

and remained constant for each test. Comparing results of reference tests to samples in which pure epoxy monomer was injected isolated the effect of limited access to imidazole and/or imidazole depletion with each healing cycle. Premixing these components is not feasible for use in a vascular healing scheme since the mixture forms a solid at room temperature after approximately 36 h.

Fig. 9 shows the healing efficiency of reference TDCB fracture specimens over multiple healing cycles for samples containing either 2, 5, or 10 wt% imidazole. Samples healed with 10 wt% imidazole had healing efficiencies consistently greater than 90% for

all 6 cycles tested. For 5 wt% samples, efficiencies consistently greater than 70% were obtained. For samples with 2 wt% imidazole, healing efficiencies ranged between 40% and 65% and gradually declined with continued healing cycles. Since a reduction in healing efficiency over multiple healing cycles was not observed for the 5 or 10 wt% reference cases, the decrease in healing efficiency over multiple healing cycles for samples containing embedded imidazole in the surrounding matrix, but not in the monomer, was attributed to a lack of availability of imidazole in the vicinity of the crack during repeat healing events. Since the imidazole is

consumed in the healing reaction, once it has been depleted from the damaged region over multiple cycles, healing can no longer take place and healing performance in later healing cycles was reduced and eventually eliminated.

3.4. Scanning electron microscope fractography

Fracture surfaces of TDCB specimens containing 10 wt% 24-EMI healed over multiple cycles at 100 °C for 1 h were examined by scanning electron microscopy (Fig. 10). Virgin fracture surfaces appear clean and glassy indicating brittle failure, while healed specimens show increasing tortuosity and polymer build-up with increasing healing cycle, confirming the presence of healed material in the crack plane.

3.5. Raman spectrography

Raman spectra of samples analyzed are provided in Fig. 11a–b. In the self-healing II specimen a peak emerges at a Raman shift of 1112 cm^{-1} which is absent in all control specimens. This peak is consistent with previously observed spectra corresponding to the creation of an aliphatic ether bond typical of etherification mechanisms present during anionic polymerization of epoxides using imidazole initiators [48]. This peak is also strongly present in the premixed healed specimen, confirming the proposed healing mechanism depicted in Fig. 11c.

All samples fabricated using the EPON 862/Epikure 3300 matrix system have a strong peak at 1050 cm^{-1} corresponding to the presence of a tertiary amine typical of epoxy/amine cross-linked polymers [53]. This peak is not present in the premixed healed specimen, however, since the polymerized product formed through the epoxy/imidazole reaction contains no tertiary amines.

4. Conclusions

In this work the healing performance and mechanical properties of a novel self-healing epoxy matrix system was evaluated. Healing was achieved by incorporating 2-ethyl-4-methylimidazole (24-EMI) into a host epoxy matrix for use as a latent anionic polymerization initiator of an epoxy monomer healing agent that was manually delivered. DSC testing confirms that adduct formation between the host epoxy matrix and embedded 24-EMI occurs during initial fabrication. This reaction leads to a decrease in the glass transition temperature and an increase in fracture toughness of the host epoxy with increasing initiator content. Confocal Raman spectra confirm the proposed healing mechanism. Evaluation of self-healing performance using tapered double cantilever beam (TDCB) specimens demonstrated greater than 90% healing efficiency in samples containing 10 wt% 24-EMI. Reducing the concentration of 24-EMI resulted in lower healing efficiencies because of incomplete healing agent polymerization, as confirmed by isothermal DSC testing. Degradation of self-healing performance with each fracture-healing cycle is due in part to hindered access to 24-EMI in the vicinity of the crack and its consumption during each healing cycle. Nonetheless, samples containing 10 wt% imidazole demonstrate up to 11 healing cycles with near 100% recovery through the first 3 cycles. In addition, reasonable healing efficiencies (ca. 60%) are obtained for samples healed for 36 h at 60 °C demonstrating significant reductions in the required temperature for latent self-healing using our imidazole-based scheme.

Acknowledgments

The authors gratefully acknowledge funding support from the U.S. Army Research Laboratory (grant number W911NF-14-

2-0003). Authors also acknowledge Ke Yang, Dr. Maxwell Robb, and Dr. Charles Deisendruck for assistance in DSC measurements and insightful chemistry discussions as well as Dr. Amanda Jones for discussion of TDCB specimen design and testing. Electron microscopy and Raman spectra collection was performed in the Imaging Technology Group at the Beckman Institute for Advanced Science and Technology at the University of Illinois with the assistance of Dr. Scott Robinson and Dr. Dianwen Zhang.

References

- [1] Blaiszik BJ, Kramer SLB, Olugebefola SC, Moore JS, Sottos NR, White SR. Self-healing polymers and composites. *Annu Rev Mater Res* Jun. 2010;40(1):179–211.
- [2] Toohey KS, Hansen CJ, Lewis JA, White SR, Sottos NR. Delivery of two-part self-healing chemistry via microvascular networks. *Adv Funct Mater* May 2009;19(9):1399–405.
- [3] Hansen CJ, Wu W, Toohey KS, Sottos NR, White SR, Lewis JA. Self-healing materials with interpenetrating microvascular networks. *Adv Mater* Nov. 2009;21(41):4143–7.
- [4] Hansen CJ, White SR, Sottos NR, Lewis JA. Accelerated self-healing via ternary interpenetrating microvascular networks. *Adv Funct Mater* Nov. 2011;21(22):4320–6.
- [5] Hamilton AR, Sottos NR, White SR. Self-healing of internal damage in synthetic vascular materials. *Adv Mater* Dec. 2010;22(45):5159–63.
- [6] Hamilton AR, Sottos NR, White SR. Pressurized vascular systems for self-healing materials. *J R Soc Interface* May 2012;9(70):1020–8.
- [7] Hamilton AR, Sottos NR, White SR. Mitigation of fatigue damage in self-healing vascular materials. *Polymer* Nov. 2012;53(24):5575–81.
- [8] Patrick JF, Sottos NR, White SR. Microvascular based self-healing polymeric foam. *Polymer* Aug. 2012;53(19):4231–40.
- [9] Dry C. Procedures developed for self-repair of polymer matrix composite materials. *Compos Struct* Jul. 1996;35(3):263–9.
- [10] Pang JWC, Bond IP. ‘Bleeding composites’—damage detection and self-repair using a biomimetic approach. *Compos Part Appl Sci Manuf* Feb. 2005;36(2):183–8.
- [11] Pang JWC, Bond IP. A hollow fibre reinforced polymer composite encompassing self-healing and enhanced damage visibility. *Compos Sci Technol* Sep. 2005;65(11–12):1791–9.
- [12] Bley S, Loader C, Hawyes V, Humberstone L, Curtis P. A smart repair system for polymer matrix composites. *Compos Part Appl Sci Manuf* Dec. 2001;32(12):1767–76.
- [13] Trask RS, Bond IP. Biomimetic self-healing of advanced composite structures using hollow glass fibres. *Smart Mater Struct* Jun. 2006;15(3):704–10.
- [14] Williams G, Trask R, Bond I. A self-healing carbon fibre reinforced polymer for aerospace applications. *Compos Part Appl Sci Manuf* Jun. 2007;38(6):1525–32.
- [15] Trask RS, Williams GJ, Bond IP. Bioinspired self-healing of advanced composite structures using hollow glass fibres. *J R Soc Interface* Apr. 2007;4(13):363–71.
- [16] Norris CJ, Bond IP, Trask RS. Interactions between propagating cracks and bioinspired self-healing vasculature embedded in glass fibre reinforced composites. *Compos Sci Technol* Apr. 2011;71(6):847–53.
- [17] Norris CJ, White JAP, McCombe G, Chatterjee P, Bond IP, Trask RS. Autonomous stimulus triggered self-healing in smart structural composites. *Smart Mater Struct* Sep. 2012;21(9):094027.
- [18] Norris CJ, Bond IP, Trask RS. Healing of low-velocity impact damage in vascularised composites. *Compos Part Appl Sci Manuf* Jan. 2013;44:78–85.
- [19] Huang C-Y, Trask RS, Bond IP. Characterization and analysis of carbon fibre-reinforced polymer composite laminates with embedded circular vasculature. *J R Soc Interface* Aug. 2010;7(49):1229–41.
- [20] Norris CJ, Meadway GJ, O’Sullivan MJ, Bond IP, Trask RS. Self-healing fibre reinforced composites via a bioinspired vasculature. *Adv Funct Mater* Oct. 2011;21(19):3624–33.
- [21] Norris CJ, Bond IP, Trask RS. The role of embedded bioinspired vasculature on damage formation in self-healing carbon fibre reinforced composites. *Compos Part Appl Sci Manuf* Jun. 2011;42(6):639–48.
- [22] Trask RS, Bond IP. Bioinspired engineering study of plantae vasculature for self-healing composite structures. *J R Soc Interface* Jun. 2010;7(47):921–31.
- [23] Esser-Kahn AP, Thakre PR, Dong H, Patrick JF, Vlasko-Vlasov VK, Sottos NR, et al. Three-dimensional microvascular fiber-reinforced composites. *Adv Mater* Aug. 2011;23(32):3654–8.
- [24] Patrick JF, Hart KR, Krull BP, Diesendruck CE, Moore JS, White SR, et al. Continuous self-healing life cycle in vascularized structural composites. *Adv Mater* 2014;26:4302–8.
- [25] Peterson AM, Jensen RE, Palmese GR. Reversibly cross-linked polymer gels as healing agents for epoxy-amine thermosets. *ACS Appl Mater Interfaces* 2009;1(5):992–5.
- [26] Peterson AM, Jensen RE, Palmese GR. Room-temperature healing of a thermosetting polymer using the Diels–Alder reaction. *ACS Appl Mater Interfaces* 2010;2(4):1141–9.

- [27] Pratama PA, Sharifi M, Peterson AM, Palmese GR. Room temperature self-healing thermoset based on the Diels–Alder reaction. *ACS Appl Mater Interfaces* 2013;5(23):12425–31.
- [28] Pratama PA, Peterson AM, Palmese GR. Diffusion and reaction phenomena in solution-based healing of polymer coatings using the Diels–Alder reaction. *Macromol Chem Phys* 2012;213(2):173–81.
- [29] Peterson AM, Jensen RE, Palmese GR. Thermoreversible and remendable glass–polymer interface for fiber-reinforced composites. *Compos Sci Technol Mar.* 2011;71(5):586–92.
- [30] Peterson AM, Jensen RE, Palmese GR. Kinetic considerations for strength recovery at the fiber–matrix interface based on the Diels–Alder reaction. *ACS Appl Mater Interfaces* 2013;5(3):815–21.
- [31] Patel AJ, Sottos NR, Wetzel ED, White SR. Autonomic healing of low-velocity impact damage in fiber-reinforced composites. *Compos Part Appl Sci Manuf Mar.* 2010;41(3):360–8.
- [32] Blaiszik BJ, Baginska M, White SR, Sottos NR. Autonomic recovery of fiber/matrix interfacial bond strength in a model composite. *Adv Funct Mater Oct.* 2010;20(20):3547–54.
- [33] Barbero EJ, Ford KJ. Characterization of self-healing fiber-reinforced polymer-matrix composite with distributed damage. *J Adv Mater COVINA* 2007;39(4):20.
- [34] Sanada K, Itaya N, Shindo Y. Self-healing of interfacial debonding in fiber-reinforced polymers and effect of microstructure on strength recovery. *Open Mech Eng J* 2008;2:97–103.
- [35] Toohey KS, Sottos NR, Lewis JA, Moore JS, White SR. Self-healing materials with microvascular networks. *Nat Mater Aug.* 2007;6(8):581–5.
- [36] White SR, Sottos NR, Geubelle PH, Moore JS, Kessler MR, Sriram SR, et al. Autonomic healing of polymer composites. *Nature Feb.* 2001;409(6822):794–7.
- [37] Jin H, Miller GM, Sottos NR, White SR. Fracture and fatigue response of a self-healing epoxy adhesive. *Polymer Mar.* 2011;52(7):1628–34.
- [38] Jin H, Miller GM, Pety SJ, Griffin AS, Stradley DS, Roach D, et al. Fracture behavior of a self-healing, toughened epoxy adhesive. *Int J Adhes Adhes Jul.* 2013;44:157–65.
- [39] Kessler MR, White SR. Self-activated healing of delamination damage in woven composites. *Compos Part Appl Sci Manuf May* 2001;32(5):683–99.
- [40] Kessler MR, Sottos NR, White SR. Self-healing structural composite materials. *Compos Part Appl Sci Manuf Aug.* 2003;34(8):743–53.
- [41] Yin T, Rong MZ, Zhang MQ, Yang GC. Self-healing epoxy composites – preparation and effect of the healant consisting of microencapsulated epoxy and latent curing agent. *Compos Sci Technol Feb.* 2007;67(2):201–12.
- [42] Yin T, Zhou L, Rong MZ, Zhang MQ. Self-healing woven glass fabric/epoxy composites with the healant consisting of micro-encapsulated epoxy and latent curing agent. *Smart Mater Struct Feb.* 2008;17(1):015019.
- [43] Yin T, Rong MZ, Wu J, Chen H, Zhang MQ. Healing of impact damage in woven glass fabric reinforced epoxy composites. *Compos Part Appl Sci Manuf Sep.* 2008;39(9):1479–87.
- [44] Yin T, Rong MZ, Zhang MQ, Zhao JQ. Durability of self-healing woven glass fabric/epoxy composites. *Smart Mater Struct Jul.* 2009;18(7):074001.
- [45] Yuan YC, Ye Y, Rong MZ, Chen H, Wu J, Zhang MQ, et al. Self-healing of low-velocity impact damage in glass fabric/epoxy composites using an epoxy–mercaptan healing agent. *Smart Mater Struct Jan.* 2011;20(1):015024.
- [46] Xiao DS, Yuan YC, Rong MZ, Zhang MQ. A facile strategy for preparing self-healing polymer composites by incorporation of cationic catalyst-loaded vegetable fibers. *Adv Funct Mater* 2009;19(14):2289–96.
- [47] Heise MS, Martin GC. Mechanism of 2-ethyl-4-methylimidazole in the curing of the diglycidyl ether of bisphenol A. *J Polym Sci Part C Polym Lett* 1988;26(3):153–7.
- [48] Heise MS, Martin GC. Curing mechanism and thermal properties of epoxy-imidazole systems. *Macromolecules Jan.* 1989;22(1):99–104.
- [49] Heise MS, Martin GC. Analysis of the cure kinetics of epoxy/imidazole resin systems. *J Appl Polym Sci* 1990;39(3):721–38.
- [50] Brown EN. Use of the tapered double-cantilever beam geometry for fracture toughness measurements and its application to the quantification of self-healing. *J Strain Anal Eng Des* 2011;46(3):167–86.
- [51] Outwater JO, Gerry DJ. On the fracture energy, rehealing velocity and refracture energy of cast epoxy resin. *J Adhes* 1969;1(4):290–8.
- [52] Rahmathullah MAM, Palmese GR. Crack-healing behavior of epoxy–amine thermosets. *J Appl Polym Sci* 2009;113(4):2191–201.
- [53] Lin-Vien D, Colthup NB, Fateley WG, Grasselli JG. Compounds containing –NH₂, –NHR, and –NR₂ groups (Chapter 10). In: Grasselli DL-VBCGFG, editor. *The handbook of infrared and Raman characteristic frequencies of organic molecules*. San Diego: Academic Press; 1991. p. 155–78.